Chapter 2
Lifetime Prediction

2.1 Introduction

Reliability continues to be one of the critical drivers for MEMS acceptance and growth. Emerging technologies require marketplace acceptance in order to be designed into high volume and critical applications. Thus, the field of reliability physics must be approached at the most fundamental level when evaluating and predicting micromachined product field performance over the lifetime of the product. The lifetime prediction portion of the reliability program is seen in Fig. 2.1.

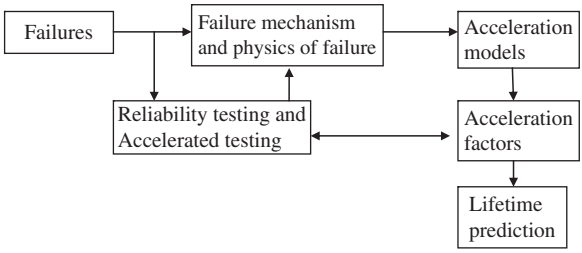

Fig. 2.1 Lifetime prediction diagram

Reliability testing is required to accelerate the lifetime of the MEMS part using acceleration factors, for proper lifetime prediction. This chapter will cover basic reliability statistics and failure distributions used in lifetime prediction.

Development of acceleration factors and reliability testing will also be covered. Case studies for two successful MEMS products, Texas Instruments' digital micro-mirror device (DLP®) and Analog Devices' accelerometer, include physics of failure, reliability testing and statistical field predictions. A third case study is a product that has yet to be put into volume production: RF MEMS.

2.2 Mathematical Measures of Reliability

This section will cover the most popular mathematical statistics used in reliability. The survivor or reliability function, cumulative distribution function, probability

A.L. Hartzell et al., *MEMS Reliability*, MEMS Reference Shelf,
DOI 10.1007/978-1-4419-6018-4_2, © Springer Science+Business Media, LLC 2011

distribution function, hazard function, and the bathtub curve concept are included and related. These functions are used to measure failure distributions and predict reliability lifetimes. The Exponential, Weibull and Lognormal distributions will be covered.

Reliability is the probability of the product performing properly under typical operating conditions for the expected lifetime intended, and an expression to define reliability is:

$$R(t) = 1 - F(t) \tag{2.1}$$

Here, $R(t)$ is the reliability function, also called the survivor function. This is defined as the probability of operating without failure to time t. $F(t)$ is the cumulative failure distribution function (CDF). In reliability, $F(t)$ is the probability that a randomly chosen part will fail by time t. A lifetime distribution model $f(t)$ is the probability density function (PDF) over the time range 0 to ∞ (infinity). The relationship between the CDF and PDF is shown in (2.2) and (2.3).

$$F(t) = \int_0^t f(t')\mathrm{d}t' \tag{2.2}$$

$$f(t) = \frac{d}{\mathrm{d}t}F(t) \tag{2.3}$$

The hazard rate $h(t)$ is also known as the instantaneous failure rate. This is the probability that failure will occur in the next time interval divided by the reliability $R(t)$ (the probability of operating without failure up to that time interval) [1].

$$h(t) = \frac{f(t)}{1 - F(t)} = \frac{f(t)}{R(t)} \tag{2.4}$$

This can also be written as

$$h(t) = -\frac{1}{R(t)}\frac{\mathrm{d}R(t)}{\mathrm{d}t} \tag{2.5}$$

Which is equivalent to

$$h(t) = -\frac{\mathrm{d}}{\mathrm{d}t}\left(\ln R(t)\right) \tag{2.6}$$

The integral of the hazard rate is the cumulative failure rate (cumulative hazard rate)

$$H(t) = \int_0^t h(t')dt = -\ln R(t) \tag{2.7}$$

The hazard rate $h(t)$ or instantaneous failure rate has dimensions of (time^{-1}). Since $R(0) = 1$ (no failures at time zero), the reliability rate over a time period t is the exponential of the cumulative hazard rate in that same time period t.

$$R(t) = \mathrm{e}^{-\int_0^t h(t')\mathrm{d}t'} \tag{2.8}$$

An important quantitative reliability concept is how long the population will survive without a failure. This is also termed mean time to failure (MTTF), more specifically, the mean-time to the first failure [2].

$$\mathrm{MTTF} = \bar{t} \equiv \int_0^\infty tf(t)\mathrm{d}t \tag{2.9}$$

2.3 Reliability Distributions

2.3.1 Bathtub Curve

The distribution of failures over the lifetime of the product population is critically important to the MEMS reliability physicist. Using these concepts, distribution functions can be developed and used for predictive purposes. A hazard rate that changes over the lifetime of the product, starting high, reducing, and increasing towards the end of the product life, is also termed the "bathtub curve" (Fig. 2.2). The population will have defective items that will fail within the first few weeks to months of the product lifetime (infant mortality) is termed the bathtub curve because of the shape of the curve itself. An ideal failure behavior is to eliminate the failures due to defects in the infant mortality portion of the curve through burn-in and/or defect reduction programs, and to not operate the product into the wear-out phase. The operational life is within the typically constant hazard rate section of the curve.

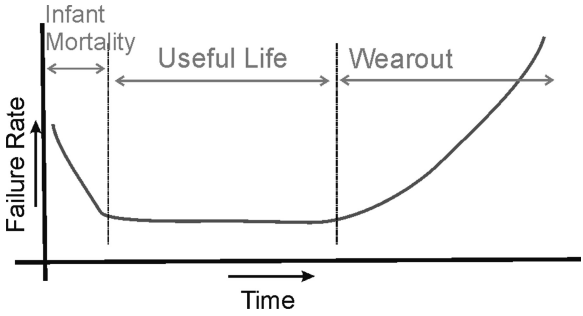

Fig. 2.2 The bathtub curve, showing three stages over the device lifetime: high initial failure due to infant mortality, constant failure rate over the useful lifetime, and increased failure rate as the devices age

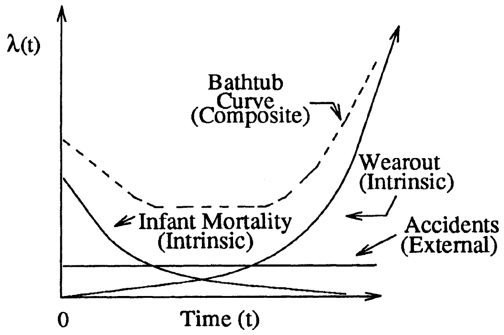

Fig. 2.3 Illustration of how the bathtub curve can be viewed as the sum of the three failure rates. Reprinted with permission. Copyright 1993 Springer Business and Media [2]

Figure 2.3 illustrates how the bathtub curve can be the composite of three failure rates: infant mortality, wear out, and externally induced failure.

For proper lifetime distribution modeling, individual failure mechanisms must be modeled independently, and there must be only one population. If there are multiple populations (or subpopulations) within the data, they must be individually extracted and statistically analyzed as single populations. There are various time to failure distributions to express population lifetime behavior statistically. Three popular statistical reliability distributions are the Exponential, the Weibull and the Lognormal.

2.3.2 Exponential Distribution

The exponential distribution is the least complex of all lifetime distribution models. The failure rate or hazard rate, $h(t)$, is λ. The failure rate is a constant in this model, which is suitable for the stable failure rate regime in Fig. 2.2, the bathtub curve. The reliability (2.10), the cumulative distribution function (CDF, (2.11)) and the probability distribution function (PDF, (2.12)) are shown below (Figs. 2.4, 2.5 and 2.6).

$$R(t) = \mathrm{e}^{-\lambda t} \tag{2.10}$$

$$F(t) = 1 - \mathrm{e}^{-\lambda t} \tag{2.11}$$

$$f(t) = \lambda e^{-\lambda t} \tag{2.12}$$

The mean time to failure of the exponential function is simply the inverse of the failure rate λ.

$$\mathrm{MTTF} = 1/\lambda \tag{2.13}$$

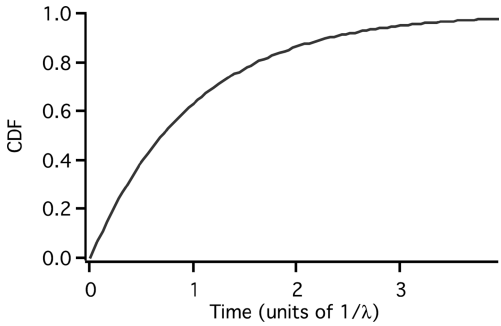

Fig. 2.4 Cumulative distribution function $F(t)$ for exponential distribution

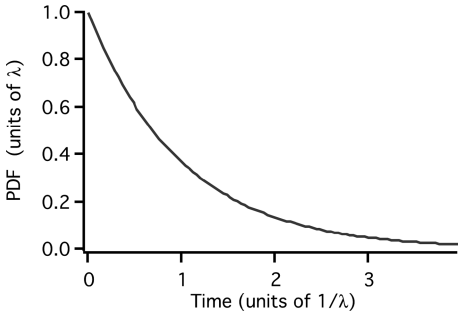

Fig. 2.5 PDF for exponential distribution

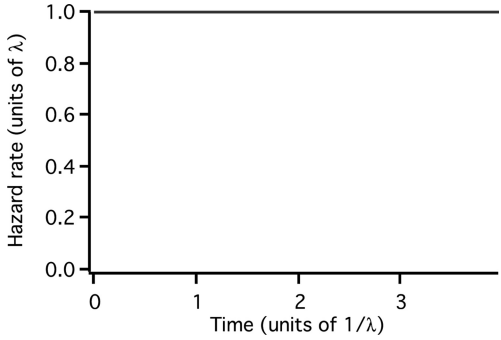

Fig. 2.6 Exponential distribution hazard rate

2.3.3 Weibull Distribution

The Weibull distribution function is used to fit various shapes of reliability curves. The Weibull function can be expressed in multiple ways [3]. The Weibull distribution expression below is the probability of survival $R(t)$ between time zero and time t [4].

$$R(t) = \mathrm{e}^{-\left(\frac{t-\gamma}{\alpha}\right)^{\beta}} \tag{2.14}$$

There are three Weibull reliability curve fit parameters in even the basic form of the Weibull function. They are (1) β, the shape parameter, (2) γ, the location parameter (also known as the defect initiation time parameter), and (3) α, the characteristic life or scale parameter. This Weibull distribution function can have two variants: the two-parameter distribution and the three-parameter distribution. The difference between the two variants is whether or not failures start at time zero. If failures do start at time zero, the defect initiation time parameter (also known as location parameter) is zero and the Weibull exponential expression is reduced to

$$R(t) = e^{-(\frac{t}{\alpha})^{\beta}} = f(t)/h(t) \tag{2.15}$$

When $\beta = 1$, equation (2.15) becomes the exponential model(2.10), with $\alpha = 1/\lambda$, the MTTF (2.13). The two parameter fit model is commonly used in reliability life predictions. The PDF of the two parameter Weibull model is in Fig. 2.7

$$f(t) = \frac{\beta}{t}\left(\frac{t}{\alpha}\right)^{\beta} e^{-(\frac{t}{\alpha})^{\beta}} \tag{2.16}$$

The CDF of the two parameter Weibull model is in Fig. 2.8 while Hazard function is in Fig. 2.9

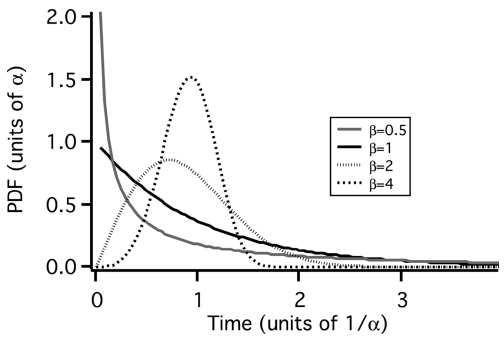

Fig. 2.7 Weibull function PDF in units of α, varying β

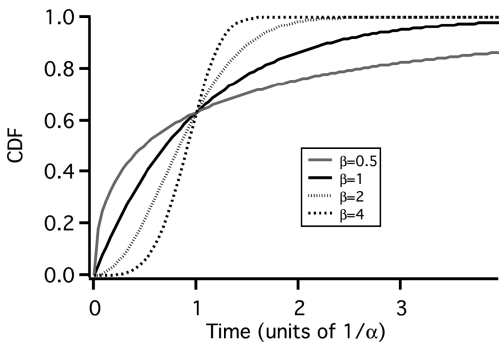

Fig. 2.8 CDF of Weibull function, varying β

$$F(t) = 1 - \mathrm{e}^{-\left(\frac{t}{\alpha}\right)^{\beta}} \tag{2.17}$$

The cumulative failure rate of the two parameter Weibull model (cumulative hazard rate) is expressed as

$$H(t) = \left(\frac{t}{\alpha}\right)^{\beta} \tag{2.18}$$

The instantaneous failure rate is

$$h(t) = \frac{\beta}{\alpha}\left(\frac{t}{\alpha}\right)^{\beta-1} \tag{2.19}$$

Sandia has published a good example of Weibull failure data on their MEMS microengine [5, 6]. In this study, 41 microengines (Figs. 2.10 and 2.11) were driven to failure with the SHiMMer test platform (Chapter 6), and the data was fit to both Weibull and lognormal functions. The cumulative failure rate is plotted as a function of accumulated cycles. A production-ready process will have a β value of 0.5 to 5 as evaluated by the Weibull function. The data in Fig. 2.11 has a β of 0.22, indicating that the data is widely dispersed. This plot shows 50% failure at 10^7 cycles.

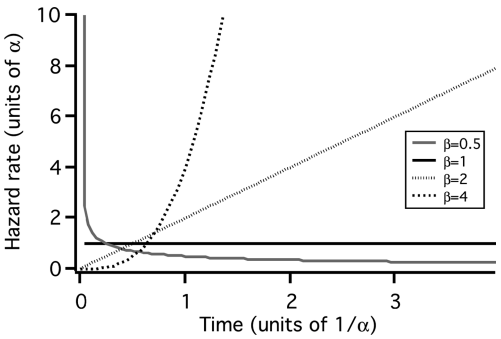

Fig. 2.9 Hazard rate for Weibull function

2.3.4 Lognormal distribution

The other popular reliability statistical distribution, the lognormal time to failure distribution, is as it is named, log normally distributed. The lognormal (also called Gaussian) distribution PDF is (Figs. 2.12 and 2.13)

$$f(t) = \frac{1}{\sigma t\sqrt{2\pi}} e^{\left(-\frac{(\ln(t)-\ln(T_{50}))^2}{2\sigma^2}\right)} \tag{2.20}$$

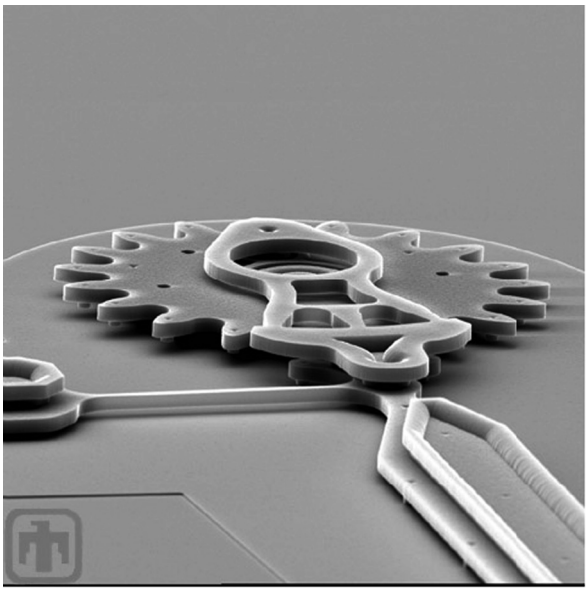

Fig. 2.10 Gear structure of Sandia's microengine, made with SUMMiT^{TM} process. Courtesy of Sandia National Laboratories, SUMMiT(TM) Technologies, www.mems.sandia.gov [6]

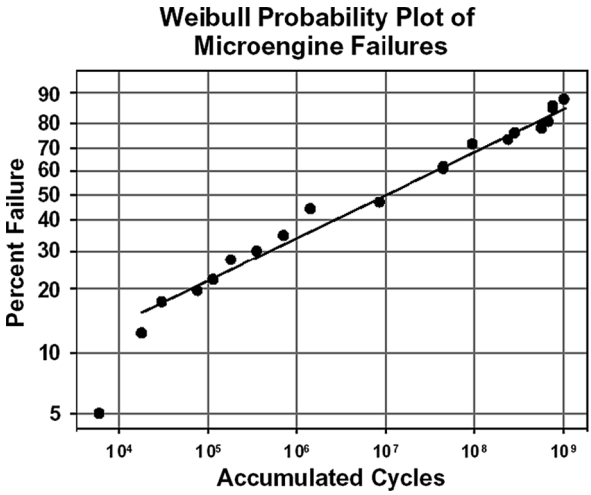

Fig. 2.11 Weibull probability plot of microengine failures. Courtesy of Sandia National Laboratories, SUMMiT(TM) Technologies, www.mems.sandia.gov [5]

The cumulative distribution function $F(t)$ is below in (2.21), while the solution is in (2.22).

$$F(t) = \int_{o}^{T} \frac{1}{\sigma t\sqrt{2\pi}} \mathrm{e}^{\left(-\frac{(\ln(t)-\ln(T_{50}))^2}{2\sigma^2}\right)} \mathrm{d}t \tag{2.21}$$

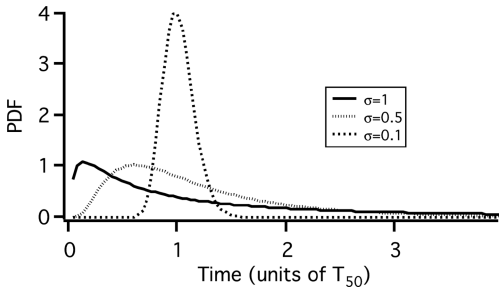

Fig. 2.12 PDF lognormal function

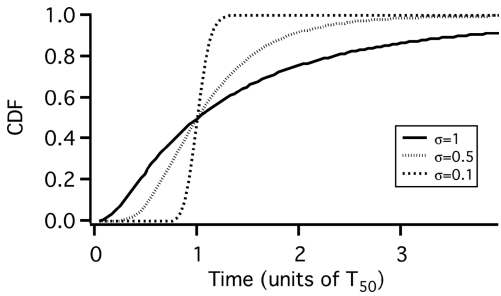

Fig. 2.13 CDF lognormal distribution

$$F(t) = \Phi\left[\frac{\ln(t/\tau)}{\sigma}\right] \tag{2.22}$$

$$\text{where } \Phi(z) = \tfrac{1}{2}\left[1 + Erf\left(z/\sqrt{2}\right)\right]$$

The shape parameter sigma σ (standard deviation) is the slope of the time to failure vs. the cumulative percent failure on a log scale. The remaining functions can be calculated using the equations in Section 2.3 (Fig. 2.14).

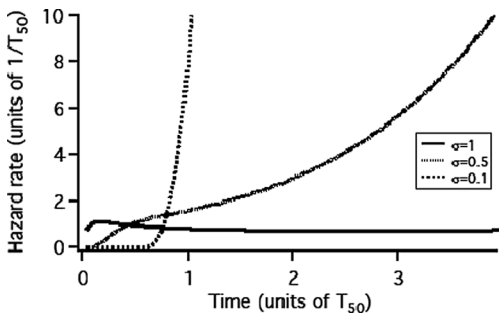

Fig. 2.14 Hazard rate for lognormal distribution

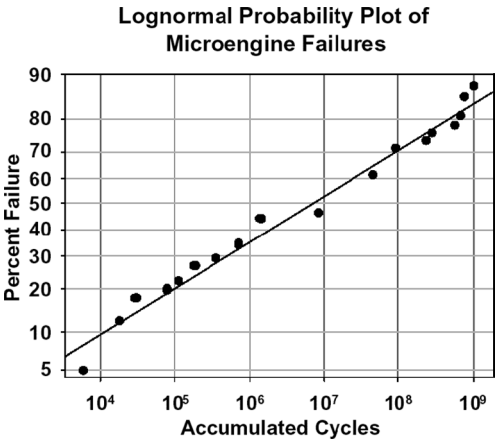

Fig. 2.15 Lognormal probability plot of sandia SUMMiT^{TM} microengine failure. Courtesy of Sandia National Laboratories, SUMMiT(TM) Technologies, www.mems.sandia.gov [5]

Figure 2.11 is the Sandia microengine failure data analyzed with the Weibull distribution function. This same data is analyzed with the lognormal function in Fig. 2.15.

In this analysis, $\sigma=5$. This indicates a large spread in the lifetime. The range typical for semiconductor products is 0.1–1. The time to 50% failure is 7.8 million cycles when this data is analyzed via the lognormal distribution.

Any analysis must be studied for bimodal distributions. This lognormal example can be also analyzed as two separate populations in Fig. 2.16. The early life failure sub-population (infant mortality in Fig. 2.2) has a time to 50% failure of 140,000 cycles while the wear-out portion of the curve has a time to 50% failure of 250

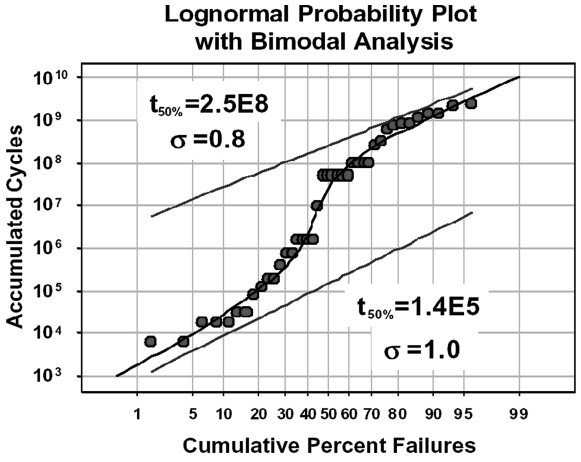

Fig. 2.16 Bimodal analysis using lognormal fit. Courtesy of Sandia National Laboratories, SUMMiT(TM) Technologies, www.mems.sandia.gov [5]

million cycles. Both of these fits have acceptable sigmas, which indicate that this analysis of the data is most accurate versus treatment as a single population.

Most failure mechanisms are treated with the lognormal distribution, but some, including solder fatigue, must be modeled with the Weibull distribution. Thus, for new physics of failure in MEMS, it is recommended to use the Weibull distribution unless it is proven that the lognormal distribution will accurately fit the shape of the empirical failure distribution.

2.3.5 Acceleration Factors

Reliability testing at accelerated conditions is critical to generating lifetime data in a much shorter period of time. Release of a reliable product to market is dependent on this concept. Stresses (examples are elevated temperature, temperature cycling, applied voltage, and relative humidity) experienced in the use environment are "accelerated", or increased to a level to accelerate the time to failure of an individual failure mechanism. The key is to create the same failure mechanism as occurs in use conditions. Development of an acceleration model is performed through knowledge of the physics of failure. An acceleration factor is calculated as compared to the use conditions. A summary table of some known MEMS failure mechanisms and accelerating stresses is below [7] in Table 2.1. Chapters 3 and 4 detail these failure mechanisms.

The field of MEMS does not have a long history of known failure models and easily obtained acceleration factors when compared to the more seasoned semiconductor industry. Standard integrated circuit reliability science has undergone many years of study to accurately predict lifetimes [8]. Table 2.2 is a chart of commonly used semiconductor packaging and assembly acceleration models [9].

There are examples in semiconductor physics of failure where many models exist for the same failure mechanism. Table 2.3 is a table that includes many existing corrosion models. The voltage term in these models must be developed as it is typically not known. In the case of established models, literature reviews are recommended to assure that the proper model is used.

To properly use acceleration models and compare to use conditions, operating environment, storage environment (non-operating) and the lifetime of the product must be known. Although this is unique to each product development effort and requires a discussion between the customer and supplier, Table 2.4 is a guideline [9] developed for the semiconductor community that can be applied to MEMS products. Examples of some major market segments are:

- Indoor: Computers, Laboratory test equipment, Projectors, Printers, etc.
- Consumer Portable: Cell phones, PDA's, Portable Laptop and Notebook PCs, etc.
- Other: Automotive, Outdoor telecommunications equipment,

Table 2.1 Examples of MEMS failure mechanisms and accelerating factors

Failure mechanism	Accelerating factors	Additional comments
Cyclic fatigue	No. of cycles, maximum applied strain, humidity	Models exist for this failure mechanism in mechanical engineering texts and literature, as well as some MEMS structures.
Creep (plastic deformation)	Temperature, applied strain	Well understood materials science field.
Stiction	Humidity, shock, vibration	Difficult to model. Surface conditions are critical.
Shorting and open circuits	Electric field, temperature, humidity	Well understood field, yet the geometries in MEMS and materials used could make this difficult to model for some structures. Again, processing effects can be critical.
Arcing	Electric field, gas pressure, gas composition	Small gaps are prone to this in specific environments. Breakdown voltage relationships should be investigated.
Dielectric charging	Electric field, temperature, radiation, humidity	Some MEMS structures such as RF MEMS are particularly susceptible to this.
Corrosion	Humidity, voltage, temperature	Polarity is important if accelerating anodic corrosion.
Fracture due to shock and vibration	Acceleration, frequency (resonance), vacuum	Models exist for this failure mechanism in mechanical engineering texts and literature, as well as some MEMS structures. Micro-scale materials properties are needed.

Not included here are extreme use environments such as space [10]. (A section on space radiation physics of failure is in Section (4.4.1).) Standards for space missions and other extreme environment MEMS applications exist, yet qualification testing for space is typically mission-specific. Standards for general qualification testing are covered in Chapter 6.

Table 2.2 Table of commonly used packaging and assembly acceleration models for semiconductors

Mechanism	Model	Assumptions
Temperature, humidity mechanisms	Peck's $TF = A_0 \times RH^{-N} \times \exp[E_a/kT]$ AF (ratio of TF values, use/stress) $AF = (RH_{Stress}/RH_{use})^{-N} \times \exp[([E_a/k)(1/T_{use} - 1/T_{stress})]$ When calculating variables that stay constant between Stress 1 and Stress 2 they will drop out of the equation.	• AF = acceleration factor • TF = time to failure • A_o = arbitrary scale factor • V = Bias voltage • RH = relative humidity as % • N = an arbitrarily determined constant • E_a = activation energy for the mechanism (0.75 eV is conservative) • k = Boltzmann's constant, 8.162×10^{-5} eV/°K • T = temperature in Kelvin. There are other models for THB mechanisms and they should be checked for the fit to the data.
Thermal effects	Arrhenius $TF = A_0 \times \exp[E_a/kT]$ AF (ratio of TF values, use/stress) $AF = Exp[(E_a/k](1/T_{use} - 1/T_{stress})]$	• AF = acceleration factor • TF = time to failure • A_o = arbitrary scale factor • E_a = activation energy for the mechanism (0.75 eV is conservative) • k = Boltzmann's constant, 8.162×10^{-5} eV/°K • T = temperature in Kelvin
Thermo-mechanical mechanisms	Coffin-Manson $N_f = C_0 \times (\Delta T)^{-n}$ AF (ratio of N_f values per stress cycle, stress/use) $AF = N_{use}/N_{stress} = (\Delta T_{stress}/\Delta T_{use})^n$	• AF = acceleration factor • N_f = number of cycles to failure • C_o = a materials dependent constant • ΔT = entire temperature cycle-range for the device • n = empirically determined constant • Assumes the stress and use ranges remain in the elastic regime for the materials • The Norris Lanzberg modification to this model takes into account the stress test cycling rate

Table 2.2 (continued)

Mechanism	Model	Assumptions
Creep	$TF = B_0(T_0 - T)^{-n} \exp(E_a/kT)$ AF (ratio of TF values, use/stess) = $((T_0 - T_{accel})/(T_0 - T_{use}))^{-n}$ $\exp([E_a/k](1/T_{accel} - 1/T_{use}))$	• AF = acceleration factor • TF = time to failure, • B_o = process dependent constant, • T = temperature in K • T_o = stress free temperature for metal (~metal deposition for temperature aluminum) • $n = 2 - 3$, (n usually ~5 if creep, thus implies $T < T_m/2$) • E_a = activation energy = 0.5 – 0.6 eV for grain-boundary diffusion, ~ 1 eV for intra-grain • k = Boltzmann's constant – 8.625 10^{-3}eV/K

Table 2.3 Various corrosion models [8]

Model	Form	Terms
Reciprocal exponential model	$TF = C_o \exp[b/RH] f(V) \exp[Ea/kT]$	C_o = arbitrary scale factor, b = ~300 Ea = 0.3 eV, $f(V)$ = an unknown function of applied voltage
Power law (Peck) model	$TF = A_o RH^{-N} f(V) \exp[Ea/kT]$	A_o = arbitrary scale factor N = ~2.7, Ea = 0.7–0.8 eV (appropriate for aluminum corrosion with chlorides are present) $f(V)$ = an unknown function of applied voltage
Exponential model	$TF = B_o \exp[(-a)\ RH] f(V) \exp[Ea/kT]$	B_o = arbitrary scale factor, a = 0.10–0.15 per %RH, Ea = 0.7–0.8 eV, $f(V)$= an unknown function of applied voltage
RH^2 (Lawson) model	$TF = C_o\ RH^2 f(V) \exp\ [Ea/kT]$	C_o = arbitrary scale factor, (typical value 4.4×10^{-4}) RH = Relative humidity as % (100% = saturated), Ea = 0.64 eV, $f(V)$ = an unknown function of applied voltage

Table 2.4 Guideline of use and storage conditions for some major market segments

Major market segment	Indoor	Consumer portable	Other
Operating life	5–10 years	5–10 years	7–25 years
Power on (hrs/week)	60–168	60–168	20–168
Cycles/day	Env. cycle: 1–2 Power cycle: 2–4	Env. cycle: 2–4 Power cycle: 4–6	Env. cycle: 2–4 Power cycle: 2–10
Moisture at low power	30–36ºC @ 85–92% RH	30–36ºC @ 85–92% RH	30–36ºC @ 85–92% RH
Operating temperature (ambient in enclosure)	0–40ºC	−18 to 55C	−55 to 125°C
Storage temperature	−40 to 50ºC	−40 to 55ºC	−40 to 55ºC

Lifetime predictions require:

- Knowledge of environmental (operating and non-operating), lifetime of end product, and manufacturing use conditions such as subsequent processing steps (packaging, printed circuit boards).
- End product packaging and application.
- Customer's acceptable failure rate over the lifetime of the product.
- Stress conditions necessary to identify failure mechanisms.
- Acceleration testing and models for lifetime prediction.
- Statistical manipulation of failure distributions in reliability testing.

When using acceleration data to predict lifetimes with acceleration models, one must assume that the shape of the curve is the same in the accelerated condition as in the use condition. The case studies at the end of this chapter illustrate various methods used for reliability lifetime prediction.

2.3.6 Lifetime Units

Failure rates are typically also reported in two popular units, FITS and ppm failure. The unit of FITS is defined as the number of failures in 10^9 device-hours. The ppm unit, which is short for parts-per-million, is always given over a stated time interval. The FITS unit is a rate of failure, while the ppm is a cumulative amount of failures out of a known population over a specific time period. The Chi-Squared method of lifetime (FIT) prediction allows cumulative data collected with specific samples to be applied to the broader population of the same design type, and allows this prediction with zero failures (assuming a constant failure rate $h(t)$ in the bathtub curve in Fig. 2.2). Here χ^2 is the Chi-Squared statistical confidence factor (a constant) that is unique for each confidence interval and number of failures in the testing while SS is sample size. Chi-squared confidence factor charts are typically presented as degrees of freedom versus confidence interval; Table 2.5 contains the statistical confidence factor χ^2 as a function of number of failures (F). To calculate the FIT rate for confidence intervals in addition to 60 and 90%, see [11] where degrees of freedom are (2F+2).

$$\text{FIT} = \frac{\chi^2}{2} \times \frac{10^9}{\text{SS} \times \text{hours}} \tag{2.23}$$

It is important to run accelerated testing properly and bring parts to failure. It is ideal statistically to bring all parts tested to failure, yet this is often an impractical use of company resources. The time to failure of the entire population (or most of it), for one individual failure mechanism, can be modeled for lifetime prediction using the statistical concepts covered in this chapter.

Table 2.5 Chi-squared constants for 60 and 90% confidence intervals

No. of failures	χ^2, 60% Conf.	χ^2, 90% Conf.
0	1.83258	4.60516
1	4.04463	7.779438
2	6.210752	10.644618
3	8.350522	13.361582
4	10.47323	15.987198
5	12.58383	18.54934
6	14.6853	21.064168
7	16.77952	23.541838
8	18.86789	25.989432
9	20.95138	28.411962
10	23.03067	30.81329
11	25.10634	33.19626
12	27.17889	35.563176
13	29.24862	37.915968
14	31.31586	40.256058
15	33.38085	42.584768

2.4 Case Studies

2.4.1 Texas Instruments Digital Mirror Device

Perhaps the field's most successful MEMS reliability story is that of the Digital Mirror Device® developed and manufactured by Texas Instruments for the Digital Light Processing® product. The reliability scientists at Texas Instruments had to start from the very beginning. There was no data on the mirror structures they had designed and fabricated, no acceleration models, and no well understood physics of failure. How does the MEMS reliability engineer start from scratch?

For new MEMS products, the test to failure approach is recommended, coupled with FMEA (Failure Modes and Effects Analysis, see Chapter 5). FMEA is a tool that is used in design and processing of parts, and can be applied to reliability as well. Various methods of collecting data for reliability are highlighted through the FMEA process.

Some background is given on the Texas Instruments product to foster discussion on failure mechanisms and accelerated testing. The failure mechanism we focus on here was hinge memory, also simply known as creep. Creep in metals is a complex mechanism that is a function of stress, temperature, whether the stress is cyclic or steady-state, and the melting temperature of the metal under study. Creep occurs in metals under constant stress and results in plastic deformation.

To determine how the metal will creep, a deformation mechanism map is helpful. The homologous temperature plotted versus the ratio of the shear stress σ_s over the shear modulus μ provides the basis for a deformation mechanism map (Fig. 2.17) [12]. The homologous temperature is defined as the ratio of the test temperature

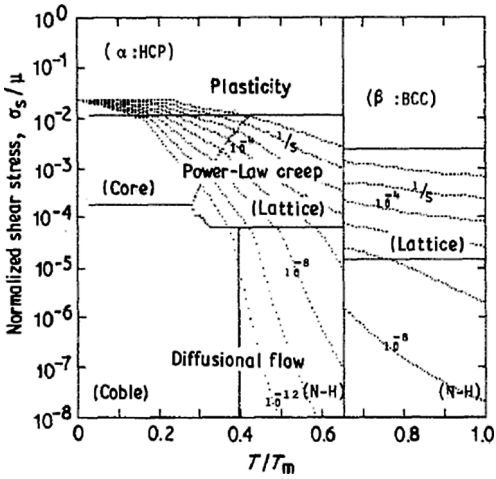

Fig. 2.17 Deformation mechanism map of homologous temperature versus normalized shear stress for a Ti-6 wt%/Al alloy with an average grain size of 100 μm. Reprinted with permission. Copyright 1991 Springer Science & Business Media [12]

of the material studied to its melting point [13]. If the material under study has an established deformation mechanism map and it applies to the MEMS structure geometries, this is a helpful start in understanding and modeling the specific creep mechanism causing failure. More detail on creep in MEMS is given in Chapter 4, Section 2.3.

Here, a value of $\sigma_s/\mu < 10^{-4}$ is where diffusional creep occurs. At low homologous temperatures, Coble creep dominates, and as homologous temperature increases, Nabarro-Herring creep occurs. These deformation mechanism maps are a function of the grain size and alloy under study, thus, processing conditions are very important to creep prediction. Figure 2.17 also has creep strain rates superimposed over the deformation map. The concept of deformation maps was initially suggested by Weertman [14–16] and was developed by Ashby and co-workers [17, 18].

Often MEMS products are so unique that standard automated (or manual) test equipment does not exist (see Chapter 6). Texas Instruments (TI), like many MEMS developers, had to build their own test stations. Using these test stations, parametric definitions of population behavior, or goodness of parts, was measured on every lot (Fig. 2.18).

The TI DMD mirror structure is a hinge/yoke structure (Fig. 2.19). The mirror is tilted and touches the surface below with a spring tip [19]. This touching action is called “landing”.

The Texas Instruments mirror is made up of various layers. An early depiction of the structure is outlined next [20].

This is shown for the reader to understand the complexity of the mechanical structure. The entire assembly sits on a CMOS memory chip. The mirror is not silicon based as many MEMS structures are, but is aluminum based. The mirror receives its voltage for electrostatic actuation through the CMOS chip via contacts etched into the structure. Voltages can be applied that result in the voltage mirror

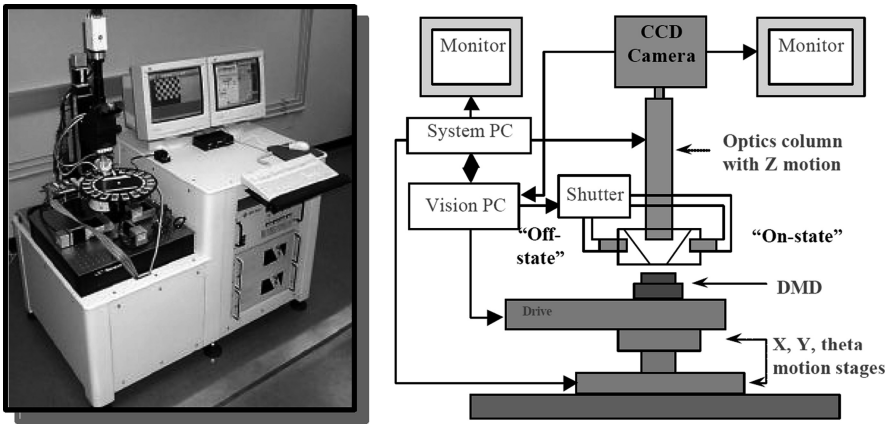

Fig. 2.18 DMD test station. Reprinted with permission. Copyright 2003 SPIE [19]

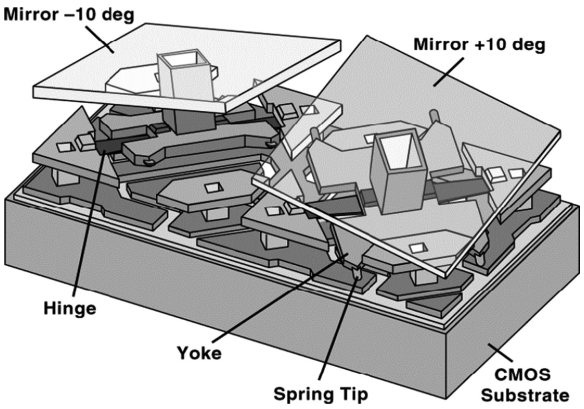

Fig. 2.19 Illustration of two landed DMD Mirrors. Reprinted with permission. Copyright 2003 SPIE [19]

"landing" as seen in Fig. 2.19. Stepped voltages and bipolar reset were included to enhance dynamic control. For more detail on this concept, see references 20 and 21 (Fig. 2.20).

Characterization by bringing parts to failure is a good initial method to determine how a MEMS structure will fail. This method was employed to generate data on which TI mirror designs and processes were most robust. Using the DMD test station, Bias/Adhesion Mirror Mapping (BAMM) Landing Curves were generated [18] upon initial performance and over time (Fig. 2.21). The method of varying one parameter at a time to understand its effect was initially used. Voltage curves were produced by applying voltage to many mirrors and collecting this data to get a distribution of the voltage range for landing. It is likely that voltage was chosen as processing and design variations can result in layer to layer thickness variations, for example, that could result in a range of voltages required for mirror landing. For any unique MEMS design and process, choosing the primary parameters to track is

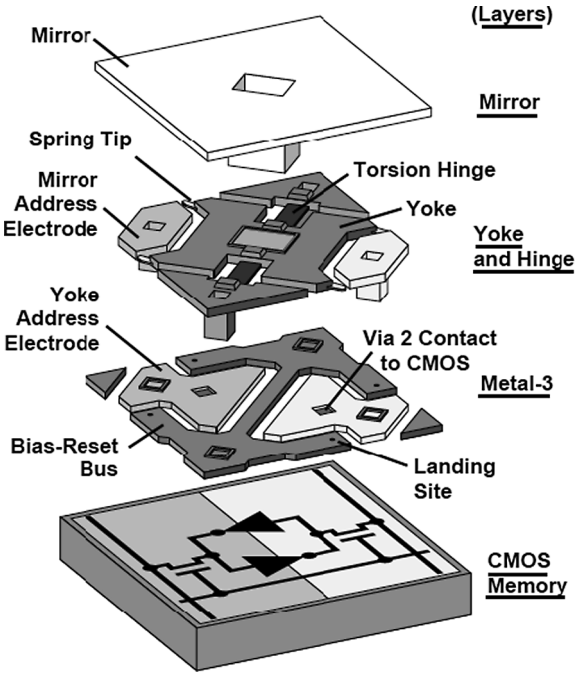

Fig. 2.20 Exploded view of early TI DMD. Reprinted with permission. Copyright 1998 IEEE [20]

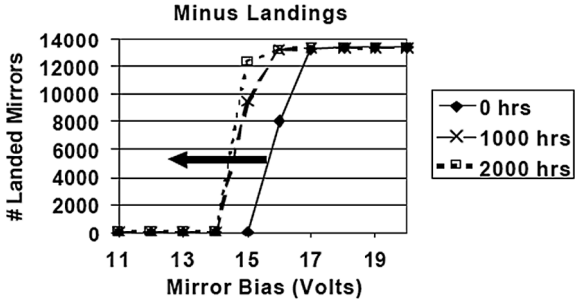

Fig. 2.21 BAMM landing curves example. Reprinted with permission. Copyright 2003 SPIE [19]

critical to the learning process. Operating parameters are often chosen initially as they need to be specified for field usage.

The change in the landing curve bias voltage over time is a clue to a change in the performance of the device. If the mirror bias changes over time, the voltage applied for landing could move out of the operating range and a failure can occur during the lifetime of the product. Thus, the reliability physics of this mechanism was studied and understood, and acceleration techniques were used to gather data in a faster manner. Figure 2.22 is an example of the work done by the Texas Instrument engineers and scientists in not only understanding the landing curve bias change, but in accelerating it as well.

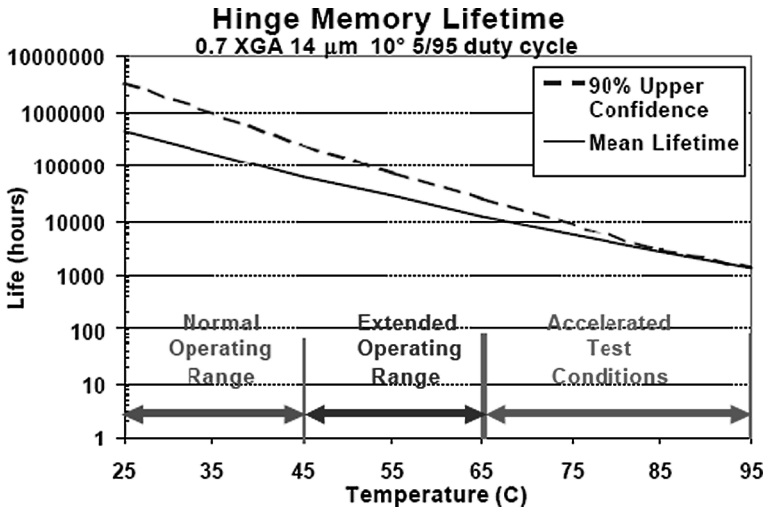

Fig. 2.22 Lifetime curve obtained by Texas Instruments. Reprinted with permission. Copyright 2003 SPIE [19]

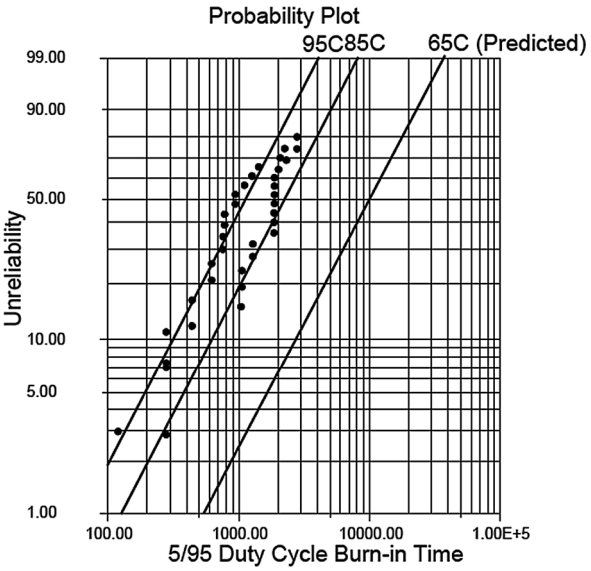

Fig. 2.23 Weibull probability plot at worse case duty cycle as a function of temperature, with lifetime predictions at maximum use temperature. Reprinted with permission. Copyright 2002 IEEE [21]

The mechanism for change in the bias voltage was termed "hinge memory" which is a creep mechanism with contribution from surface effects [21]. Creep is known to be accelerated by temperature, thus, stress testing at elevated temperature was performed. Weibull statistics were obtained (Fig. 2.23) and acceleration models were obtained for the failure mechanism. In the case of temperature stresses, the

Arrhenius model is used as the acceleration model and to determine the acceleration factor A_F (Equation (2.24)), this is industry standard in both semiconductors and MEMS. In using the following model for temperature acceleration, empirical work must be performed to determine the activation energy for the specific failure mechanism and materials set. In the case of the hinge memory failure mechanism, the activation energy (Ea) was ≥ 0.78 eV [21]. In Fig. 2.19, prediction at the maximum operating temperature of 65°C was performed using the model below, and was compared with data collected through accelerated temperature testing.

$$A_F = e^{Ea/k((1/T_{use})-(1/T_{accel}))} \tag{2.24}$$

The acceleration factor will be calculated. Using equation (2.24), the acceleration temperatures of 85°C and the use temperature of 65°C, the activation energy of 0.78 eV, and Boltzmann's constant 8.617×10^{-5} eV/°K, equation (2.24) transforms to (2.25):

$$A_F = e^{0.78\text{ eV}/8.617E-5\text{ eV/K}\left(\frac{1}{(273+65)\text{ K}}-\frac{1}{(273+85)\text{ K}}\right)} = 4.46 \tag{2.25}$$

Development of the activation energy is excellent work, yet this acceleration factor is very dependent on the proper activation energy. Table 2.6 shows the change in acceleration factor when the activation energy is slightly changed. An incorrect activation energy coupled with other use factors (duty cycle is the factor in Fig. 2.23) could greatly alter operational lifetime predictions.

Table 2.6 Acceleration factors for various activation energies using use temperature of 65°C and acceleration temperature of 85°C

Activation energy (eV)	Acceleration factor
0.6	3.16
0.65	3.48
0.7	3.83
0.75	4.21
0.78	4.46
0.8	4.64
0.85	5.11

The Texas Instruments DMD example is excellent reliability work performed to create a niche market for MEMS micromirrors. It also serves as an example to reliability physicists on how to characterize a potential failure mechanism and eliminate its effects.

2.4.2 Case Study: Analog Devices Accelerometer

The DMD example identifies how to predict lifetime for the DMD design under worst-case duty cycle as a function of temperature. An example of stiction-based

lifetime prediction as a function of mechanical shock was performed at Analog Devices on test vehicles and will be covered here. The survivor function is used, yet interestingly is a function of shock profile and not a function of time.

The Analog Devices accelerometer family is based on a differential capacitive sensing structure. Fixed and movable beams are adjacent to one another; as a mechanical shock is applied as depicted in Fig. 2.24, the movable beams move which changes the spacings between the fixed and movable beams (air gap capacitor) and results in a unique output voltage. The sensitivity of the MEMS structure, also known as the output voltage per gee-level, is a known value for each accelerometer design. Upon experiencing an externally applied mechanical shock, the shock value and pulse shape can be quantitatively determined with external algorithms (Fig. 2.25).

The Analog Devices MEMS products are amongst the highest reliability MEMS products in the world. With extremely low failure rates in the field, studies like

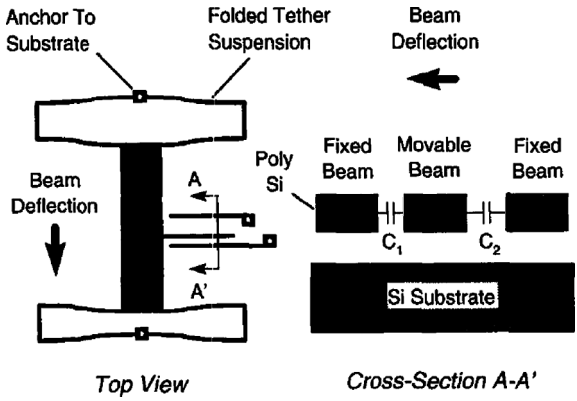

Fig. 2.24 Analog devices differential capacitive sensing MEMS structure. Reprinted from the Lancet. Copyright 1998, with permission from Elsevier [22]

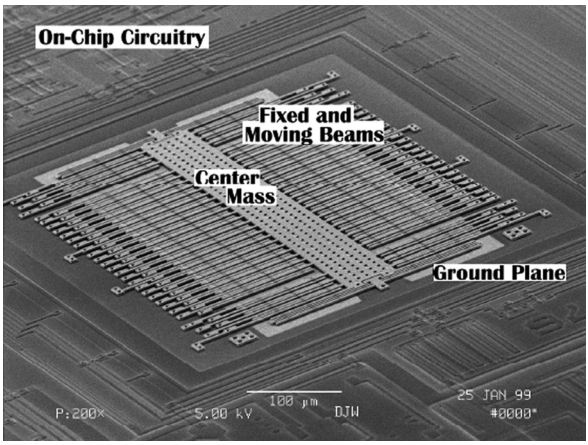

Fig. 2.25 Scanning electron micrograph of the ADXL76 Sensor structure showing the on-chip circuitry, center mass, fixed and moving beams and the ground plane. Reprinted with permission. Copyright 1999 IEEE [23]

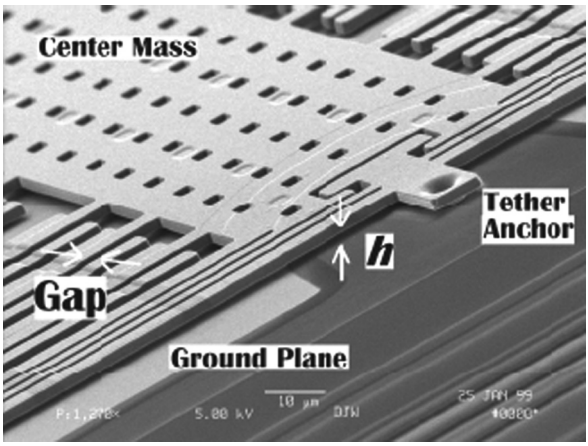

Fig. 2.26 Scanning electron micrograph showing z-axis spacing, h. Reprinted with permission. Copyright 1999 IEEE [23]

this are very difficult to perform due to the huge sample size requirements. Failures in single digit parts per million levels are typical in the field application for the Analog Devices accelerometer products [24]. In this study, a test vehicle was produced with reduced "h" spacing (Fig. 2.26) to study z-axis stiction. Typically, the restoring force of the structure would exceed the electrostatic and surface forces which would recover the device in the case of structure contact with the ground plane. Yet this test vehicle was more prone to z-axis stiction, and allowed data collection with a realistic sample size. This was an interesting study as a model could be developed to predict failure as a function of a shock profile with a relatively small number of parts.

A mechanical shock test set-up was built to test the test vehicle's stiction behavior. Figures 2.27 and 2.28 are simplified versions of the test set up required for this type of study. A shock was applied to a board-mounted packaged accelerometer test vehicle, a reference accelerometer measured the shock, and the output of the MEMS device was detected with an oscilloscope.

The failure probability of the test vehicle was determined by applying repeated mechanical shocks of various values to the parts. Since the data per part showed that stiction events were not dependent on the shock history of the part, the law of independent probabilities was used to determine the probability of failure as a

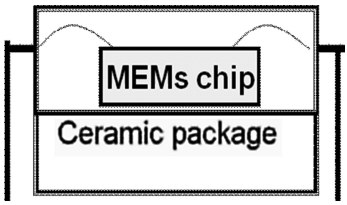

Fig. 2.27 MEMS device in ceramic package

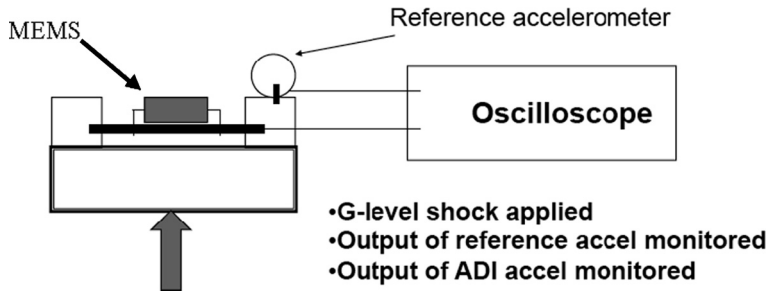

Fig. 2.28 Simplified diagram of test set up for the stiction-susceptible test vehicle

function of a series of shocks. A model was developed to predict the behavior of this population for any shock profile within the experimental mechanical shock range.

The following equation that predicts the number of failures was empirically determined from the test vehicle population [23].

$$F = q_f P_f\{G_z(s)\} \tag{2.26}$$

Here, F is predicted number of accelerometer test vehicle failures as a function of experienced mechanical shocks; q_f is the quantity of stiction-susceptible test vehicles, and $P_f\{G_z(s)\}$ is an empirically determined failure distribution (2.26). $\{G_z(s)\}$ is the z-axis lifetime shock profile that the accelerometer could theoretically experience. The survival function for this study, shown in Fig. 2.30, is related to the probability of failure as described earlier in this chapter. $P_s\{G_z(s)\}$ is the survival function as a function of mechanical shock gee level, versus in Section 2.3, where survival rate is a function of time.

$$P_f\{G_z(s)\} = 1 - P_s\{G_z(s)\} \tag{2.27}$$

$$P_s\{G_z(s)\} = P_{s1}(G_z) \times P_{s2}(G_z) \times P_{s3}(G_z) \times \cdots \times P_{sn}(G_z) \tag{2.28}$$

As an example random series of shocks can be input into the model to obtain an overall failure rate. Equation (2.27) calculates the probability of failure of the shock profile $100g$, $200g$, $300g$, $400g$, and $500g$.

$$P_f\{G_z(s)\} = 1 - [P_s\{100\,g\} \times P_s\{200\,g\} \times P_s\{300\,g\} \times P_s\{400\,g\} \times P_s\{500\,g\}] \tag{2.29}$$

The individual survival rates are taken from the empirical data polynomial fit and a final failure rate is determined.

$$P_f\{G_z(s)\} = 1 - \{(0.9809) \times (0.9636) \times (0.9481) \times (0.9344) \times (0.9225)\} \tag{2.30}$$

$$P_f\{G_z(s)\} = 0.2275 \tag{2.31}$$

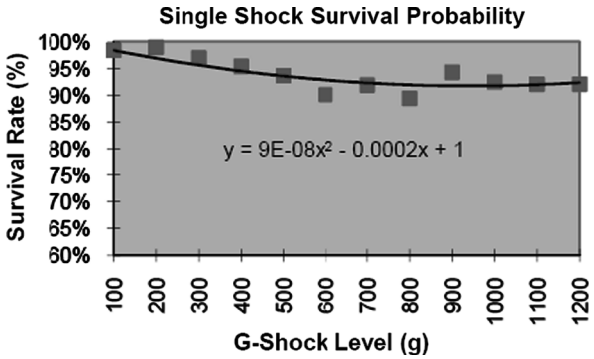

Fig. 2.29 Second order polynomial fit to mechanical shock survival data. Reprinted with permission. Copyright 1999 IEEE [23]

In the example shown the probability of failure is 22.75% for a set of test vehicles that undergoes a random series of shocks. A simple second order polynomial fit was made to the empirical data to obtain a survival rate for a single mechanical shock, this was put into the model to obtain the probability of failure for a series of shocks at various mechanical shock levels (shock profile). Figure 2.29 contains the mechanical shock survival data. A proprietary acceleration factor would next be used to apply this model to a product design for stiction prediction. For more information on mechanical shock physics of failure see Chapter 4 while stiction is covered in Chapter 3. This example shows how MEMS can change the game; mechanical failures are not always a function of time. In this case, the survival and failure rates are a function of operational lifetime mechanical shock profiles.

2.4.3 Case Study: RF MEMS

Compared to existing solid-state technologies for switching 1–40 GHz signals, RF MEMS switches offer the potential for lower insertion loss, extremely high linearity, and greatly reduced power consumption, in addition to possible integration with microwave circuits. Since the first RF MEMS switch reported in the 1970s [25], enormous progress has been made in performance and reliability. Excellent performance has been demonstrated for electrostatically operated devices [26].

Yet, unlike MEMS accelerometers and TI's DMD chips, RF MEMS have not yet found widespread acceptance, and are not a mass produced COTS (component off the shelf) part. The barrier to commercialization is partially cost, but principally long-term reliability and packaging. We shall give a brief overview of the operation principle of capacitive RF MEMS switches, then discuss the main failure mode of dielectric charging, and the research that has allowed accelerated testing of such devices.

This section will focus principally the RF switch first developed at Raytheon [27], and now being brought to market by MEMtronics Corp., for which some of the trade-offs necessary for achieving long-term reliability have been published.

There are two mains classes of RF MEMS switches: (a) ohmic switches, in which two conductors are brought into contact to close a circuit, essentially a miniaturized relay switch, and (b) capacitive switches, in which a membrane is moved to change the capacitance between the RF signal line and ground. We discuss only the capacitive switch in this section.

Figure 2.30 is a schematic cross-section of a MEMS capacitive switch. The movable membrane, generally a few hundred nm thick aluminum alloy, can be electrostatically deflected down by a few μm to rest on the thin dielectric covering the central metal conductor. Figure 2.31 provides a top view of a device from MEMtronics, on which the three horizontal conductors (ground-signal-ground) can be seen. The center conductor carries both the RF signal and the DC actuation voltage. When no voltage is applied the membrane remains in the up position, providing a small capacitance C_{off} from the signal line to ground. When a sufficiently high voltage DC is applied to the signal line, the membrane collapses on the dielectric,

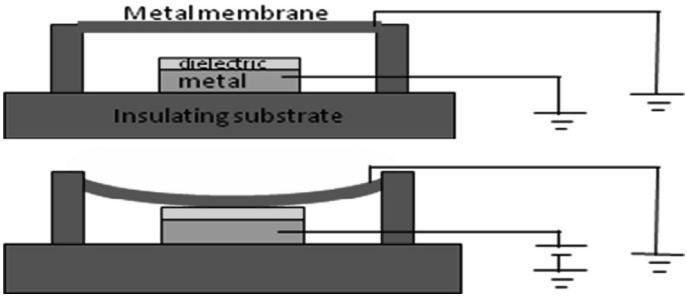

Fig. 2.30 schematic cross-section of a capacitive RF MEMS switch, *top*: undeflected (no dc bias), capacitance C_{off}, *bottom*: snapped down (bias voltage larger than $V_{\text{pull-in}}$), larger capacitance C_{on}

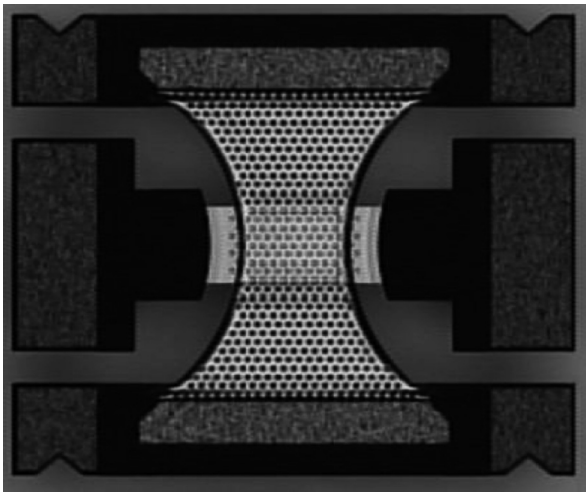

Fig. 2.31 Top view of a MEMtronics Corp RF capacitive MEMS air-gap switch on glass substrate. The membrane is the hour-glass shaped feature. The horizontal central conductor carries both the RF signal and the DC actuation voltage. Reprinted with permission. Copyright 2008 Society of Photo Optical Instrumentation Engineers [28]

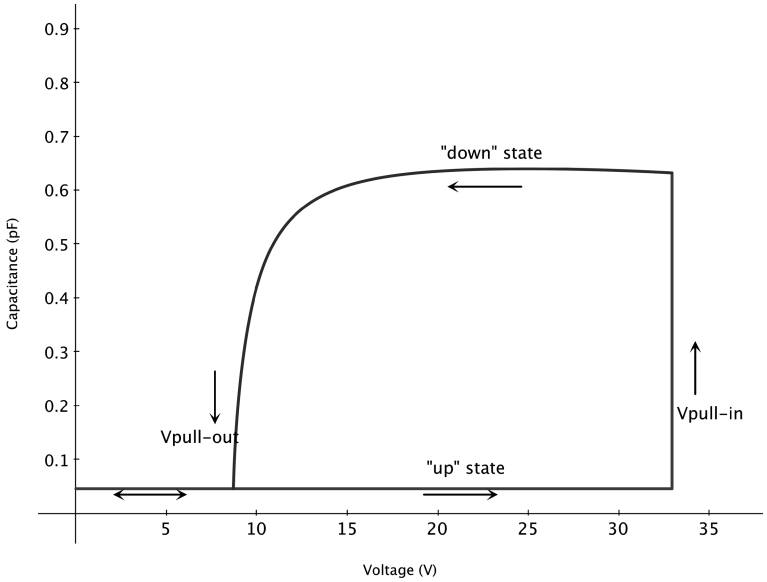

Fig. 2.32 Schematic representation of switch capacitance vs. DC voltage, showing pull-in voltage V_{pi}, pull-out voltage V_{po}, and the hysteresis in operation (which allows using a "hold" voltage much lower than the switching voltage)

providing a much greater capacitance C_{on}. The $C_{\text{on}}/C_{\text{off}}$ ratio is a good figure of merit. Device operation is illustrated in Fig. 2.32.

The main failure modes reported for this type of switch, associated accelerating factors, and possible solutions are given in Table 2.7.

Stiction will be discussed in Chapter 3, fatigue, creep and dielectric charging in Chapter 4. There is generally a trade-off involved in achieving high reliability, either leading to a small performance drop, or to an increased fabrication complexity, or to a slight increase cost due to a hermetic package for instance. For example, reducing the actuation voltage can provide orders of magnitude increase in device lifetime by reducing charging. However lower voltage operation, assuming we do not change the conductor widths as they need to present the correct impedance, requires a more compliant suspension, which leads to reduced power handling (due to self-actuation), less restoring force and hence higher susceptibility to stiction, and requires a better stress engineering if the metals.

Dielectric charging has been identified as the most important failure mechanism for this type of switch. Switch operation generally require at least 30 V, and for a typical dielectric thickness of 300 nm, this leads to an electric field of 10^8 V/m when the switch is in the down position. At such high fields, charge can readily tunnel into dielectrics and lead to trapped charge. The charge transport mode depends on the dielectric (generally Frenkel-Poole for silicon-rich Silicon nitrides, and Fowler-Nordheim for silicon oxides), but is a complex phenomenon,

Table 2.7 Capacitive RF-MEMS main failure mode and techniques that can accelerate those failure modes

Failure mode	Accelerating conditions	Possible design change
Creep of metal membrane	Temperature, RF power (leading to heating), stress in metal layer	More creep- resistant alloy, better conductor for less ohmic heating
Stiction	Humidity, surface cleanliness, surface roughness	Hermetic packaging, roughness control of membrane and dielectric
Fatigue in membrane	Number of cycles, temperature	Reduce maximum stress by geometry change, change alloy
Dielectric charging	Humidity, electric field, temperature	Lower operating voltage, change dielectric, patterned dielectric, separate signal and drive electrodes

with strong dependence on dielectric composition and deposition conditions, surface cleanliness, geometry.

Charging only occurs in this down position. It was shown that for charging is the total time in the down state, rather than the number of cycles that defines lifetime [29]. Trapped charge leads to failure either from the membrane being stuck down if the trapped charge generates a sufficient electrostatic force, or the membrane being stuck up is the trapped charge screens the applied voltage and raised V_{pi} over the normal operating point.

Dielectric charging in RF MEMS switches takes two main forms: (a) bulk charging due to charge injected into the dielectric from the bottom electrode, and (b) surface charging on top of the dielectric. [28, 30]. Bulk charge leads to a decrease in V_{pi} as the field from the charge adds to the applied field. Surface charge screens the applied voltage, leading to an increase in V_{pi}.

Surface charging is generally avoided at all cost because it shows rapid charging, but slow discharge, and has much higher charge density than bulk charge. Surface charging occurs at voltage above 45 V, and in the presence of humidity or surface contamination. So by operating at lower voltages and in a dry and clean environment, it is possible to limit charging to bulk charging. This is the approach MEMtronics have shown [28].

Using transient current spectroscopy on test structures (metal-insulator-metal structures with no moving parts as well as on working RF-MEMS switch), the MEMtronics team developed a technique to quantify charge tunneling and trapping in the dielectric [26]. This tool allowed the rapid comparison of different dielectrics, as well as the prediction of trapped charge as a function of time, voltage and duty cycle.

Solutions to minimize charging include:

- Increasing the thickness of the dielectric to reduce the applied field, at the cost of lower $C_{on.}$ If one also switches to a dielectric with a higher relative permittivity, as is done for instance for gate dielectric stacks, one could increase thickness without reducing C_{on}. This introduces processing challenges.
- Decreasing the drive voltage. Goldsmith et al. have shown a factor of 10 increase in lifetime for every 5 V reduction in drive voltage [31]. A commonly used technique is a stepped waveform, suing a high voltage for switching and a low voltage for holding the membrane down.
- Change the dielectric to one with less charge traps. For instance MEMtronics uses silicon oxide rather than silicon nitride, which was the "conventional" solution for years for RF MEMS switches. About an order of magnitude reduction in charging is seen with a suitable SiO_x dielectric for comparable C_{on}, as can be seen in Fig. 2.36 [30, 32].
- Pattern the dielectric to minimize the area where charge can accumulate. This is an effective technique, and is implemented in the device in Fig. 2.31. The tradeoff is increased lifetime for decreased C_{on}. [28]
- Hermetic or dry packaging to control humidity. This addresses principally surface charging, and has been successfully implemented [33].

Figure 2.33 shows an example of an accelerated test on a MEMtronics test vehicle, where a 35 V DC signal is used with a 100% duty cycle, showing absolute worst case charging, which appears to be surface charging as V_{pi} increases with time. By way of comparison, Fig. 2.34 is data for a similar device, but under less accelerated conditions, showing no evolution of V_{pi} with time. This type of data allows lifetime to be accurately predicted for well-defined operating conditions.

Controlling surface charge cannot be done without controlling the ambient humidity, which requires a hermetic package. For cost reasons this package must be as compact as possible, and wafer-level packaging is the accepted route, with

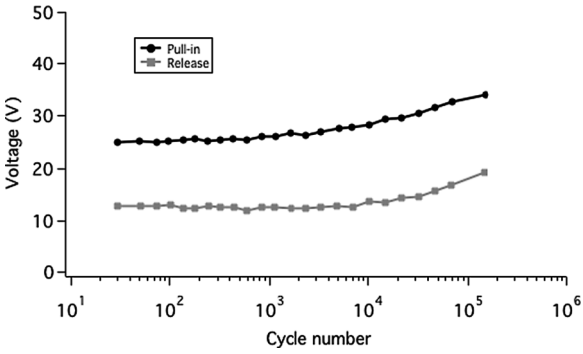

Fig. 2.33 Shift of pull-in and pull-out voltages vs. time for an RF-MEMS switch under accelerated conditions (35 V DC bias, 100% duty cycle). Reprinted with permission. Copyright 2008 Society of Photo Optical Instrumentation Engineers [28]

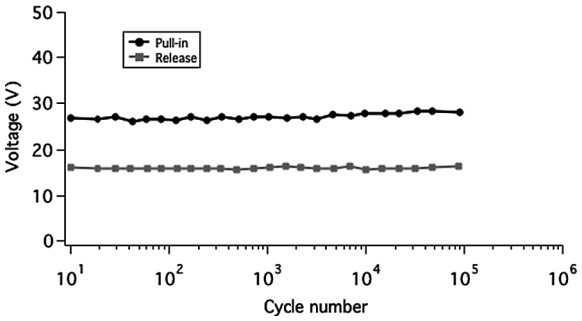

Fig. 2.34 Shift of pull-in and pull-out voltages vs. time for an RF-MEMS switch under less accelerated conditions than in Fig. 2.33. Reprinted with permission. Copyright 2008 Society of Photo Optical Instrumentation Engineers [28]

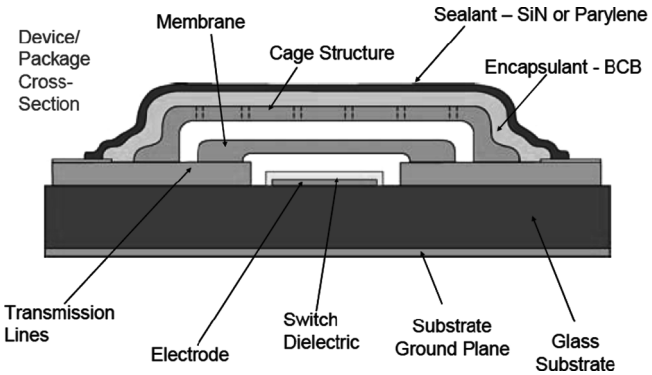

Fig. 2.35 Schematic cross-section of wafer-level packaging developed by MEMtronics to hermetically seal RF MEMS switches with minimal footprint. Reprinted with permission. Copyright 2005 ASME [33]

many different technologies having been demonstrated. The MEMtronics device uses a wafer-level packaging scheme that has a particularly small footprint, shown schematically in Fig. 2.35. The need for such ambient control is illustrated in figure where the effect of %RH is clearly seen as a shift in V_{pi}.

The packaging scheme of Fig. 2.35 was subjected to a number of accelerated lifetime cycles, using elevated temperature and elevated humidity levels to compare different sealants and encapsulants. The tests were highly accelerated (computed acceleration factor of 10^5) and so must be interpreted with care, as higher activation energy mechanisms will be much more highly accelerated, and infant mortality will be overlooked. Nevertheless, the data shown in Fig. 2.37 suggest the package will remain hermetic for over 20 years, thus ensuring surface charging will not occur over the useful life of the RF switch.

To conclude on this example of a capacitive RF MEM switch, very significant progress has been made in identifying failure modes, in determining accurate ways of accelerating those failures, and in devising ingenious solutions to ensure good lifetime while keeping the overall cost down. In-situ diagnostic tools have been

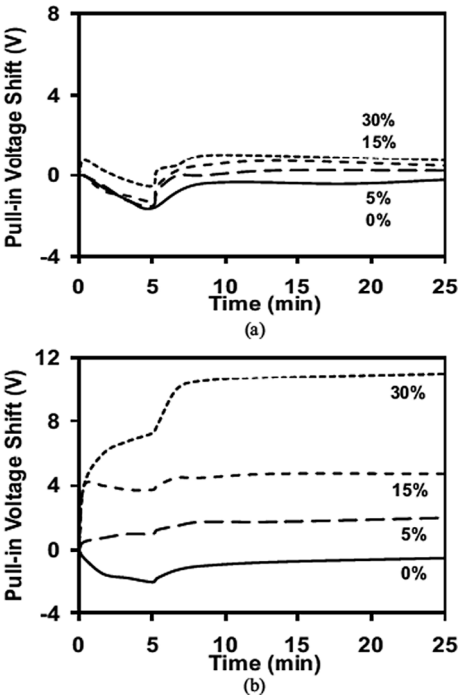

Fig. 2.36 Shift in V_{pi} after 5 min high field stress, for silicon oxide (*top*) and silicon nitride (*bottom*) for different relative humidity conditions, illustrating both the superiority of silicon oxide and the strong effect of relative humidity on surface charge. Reprinted with permission. Copyright 2009 IEEE [30]

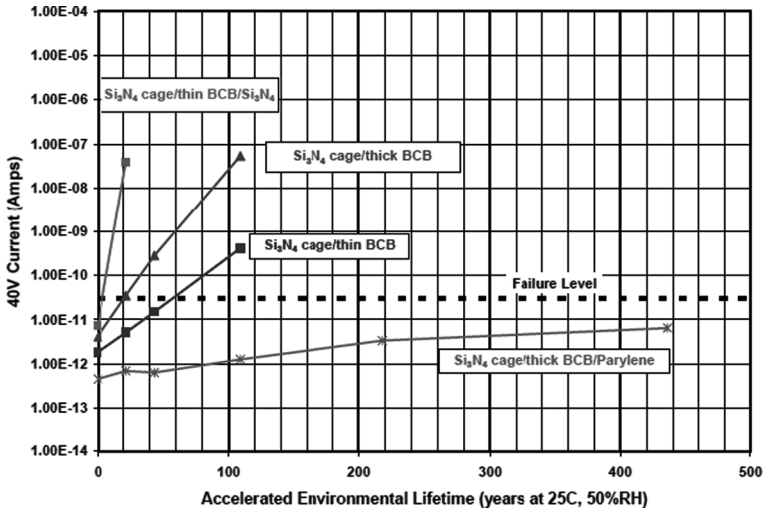

Fig. 2.37 Accelerated test data on the hermetic packaging scheme shown in Fig. 2.36 extrapolated to normal operating conditions. Reprinted with permission. Copyright 2005 ASME [33]

developed, allowing lifetime to be accurately predicted, and have shown that charging effects can be managed. One can look forward to the commercialization of RF-MEMS switches in the near future.

2.5 Summary

The importance of predictive modeling, acceleration factors, physics of failure, and separating populations for lifetime prediction is covered in this chapter. Examples of failure mechanisms include creep, stiction, and dielectric charging. Accelerated testing and test set-ups are covered through these published examples. Physics of failure is covered in more detail in Chapters 3 and 4, and MEMS test platforms are covered in Chapter 6.

References

1. Guttman, I., Wilks, S.S., Hunter, J.S. (1982) *Introductory Engineering Statistics*. New York: John Wiley and Sons.
2. Nash, F.R. (1993) *Estimating Device Reliability: Assessment of Credibility*. Dordrecht: Kluwer Academic Publishers, p. 64, Springer Publishing, now copyright holder.
3. Klinger, D., Nakada, Y., Menendez, M. eds. (1990) *AT&T Reliability Manual*. New York: Van Nostrand Reinhold.
4. Dodson, B. (2006) *The Weibull Analysis Handbook*, 2nd edn. Milwaukee: American Society for Quality, Quality Press.
5. Tanner, D.M. et al. (2000) *MEMS Reliability: Infrastructure, Test Structures, Experiments, and Failure Modes*. Sandia Report SAND2000-0091, p. 78 (Courtesy Sandia National Laboratories, Radiation and Reliability Physics Dept., www.mems.sandia.gov)
6. Courtesy of Sandia National Laboratories. SUMMiT(TM) Technologies, www.mems.sandia.gov, http://mems.sandia.gov/gallery/images.html
7. Shea, H.R. (2006) Reliability of MEMS for space applications. In V. D.M. Tanner, R. Ramesham (eds) *Reliability, Packaging, Testing, and Characterization of MEMS/MOEMS*. Proc. of SPIE Vol. 6111, 61110A.
8. Blish, R., Durrant, N. (2000) Semiconductor device reliability failure models. Int. Sematech. Technol. Transfer # 00053955A-XFR, May 31.
9. Blish, R., Huber. S., Durrant, N. (1999) Use condition based reliability evaluation of new semiconductor technologies. *International Sematech* Technology Transfer # 99083810A-XFR, August 31.
10. Planning, Developing and Managing an Effective Reliability and Maintainability (R&M) Program (1998) NASA-STD-8729.1, National Aeronautics and Space Administration, December 1998.
11. FLA (1986) *Standard Mathematical Tables*, 26th edn. Boca Raton: CRC Press, p. 548.
12. Janghorban, S. et al. (1991) Deformation-mechanism map for Ti-6 wt% Al Alloy. J. Mater. Sci. 26, 3362–3365.
13. Dieter, G.E. (1986) *Mechanical Metallurgy*. New York: McGraw-Hill, Inc.
14. Weertman, J. (1956) J. Mech Phys Sol. 4, 230.
15. Weertman, J. (1960) Trans. AIME 218, 207.
16. Weertman, J. (1963) Trans. AIME 227, 1475.
17. Ashby, M.F. (1972) Acta Met. 20, 887–897.
18. Frost, H.J., Ashby, M.F. (1982) Deformation-mechanism maps. New York: Pergamon Press.

19. Douglass, M.R. (2003) DMD reliability: a MEMS success story. In R. Ramesham, D. Tanner (eds) *Reliability, Testing and Characterization of MEMS/MOEMS II*. Proceedings of SPIE Vol. 4980, SPIE.
20. Douglass, M.R. (1998) Lifetime estimates and unique failure mechanisms of the digital micromirror device (DMD). Reliability Physics Symposium; 1998 IEEE International Volume, Issue 31.
21. Sonheimer, A. (2002) Digital micromirror device (DMD) hinge memory lifetime reliability modeling. IEEE 40th Annual International Reliability Physics Symposium, Dallas Texas.
22. Chau, K., Sulouff, R. (1998) Technology for the high-volume manufacturing of integrated surface-micromachined accelerometer products. Microelectron. J. 29, 579–586.
23. Hartzell, A., Woodilla. D. (1999) Reliability methodology for prediction of micromachined accelerometer stiction. 37th International Reliability Physics Symposium (IRPS), San Diego, California. p. 202.
24. Hartzell, A. et al. (2001) MEMS reliability, characterization, and test. In R. Ramesham (ed) *Reliability, Testing, and Characterization of MEMS/MOEMS*. Proc. SPIE Vol. 4558, pp. 1–5.
25. Peterson, K. E. (1979) Micromechanical membrane switches on silicon. IBM J. Res. Develop. 23(4), 376–385, July 1979.
26. Yuan, X., Hwang, J.C.M., Forehand, D., Goldsmith, C.L. (2005) Modeling and characterization of dielectric-charging effects in RF MEMS capacitive switches. IEEE Int. Microwave Symp. paper WE3B-3, June 2005.
27. Yao, Z.J., Chen, S., Eshelman, S., Denniston, D., Goldsmith, C. (1999) Micromachined low-loss microwave switches. J. Microelectromech. Syst. 8(2), 129–134, June 1999.
28. Goldsmith, C.L., Forehand, D., Scarbrough, D., Peng, Z., Palego, C., Hwang, J.C.M., Clevenger, J. (2008) Understanding and improving longevity in RF MEMS capacitive switches. Proc. Int. Soc. Optical Eng. 6884(03), Feb 2008
29. Van Spengen, W.M., Puers, R., Mertens, R., De Wolf, I. (2004) A comprehensive model to predict the charging and reliability of capacitive RF MEMS switches. J. Micromech. Microeng. 14(4), 514–521.
30. Peng, Z., Palego, C., Hwang, J.C.M., Moody, C., Malczewski, A., Pillans, B., Forehand, D., Goldsmith, C. (2009) Effect of packaging on dielectric charging in RF MEMS capacitive switches. IEEE Int. Microwave Symp. Dig., 1637–1640, June 2009.
31. Goldsmith, C., Ehmke, J., Malczewski, A., Pillans, B., Eshelman, S., Yao, Z., Brank, J., Eberly, M. (2001) Lifetime characterization of capacitive RF MEMS switches. IEEE Int. Microwave Symp. 1, 227–230, May 2001.
32. Peng, Z., Palego, C., Hwang, J.C.M., Forehand, D., Goldsmith, C., Moody, C., Malczewski, A., Pillans, B., Daigler, R., Papapolymerou, J. (2009) Impact of humidity on dielectric charging in RF MEMS capacitive switches. IEEE Microwave Wireless Comp. Lett. 19(5), 299–301, May 2009.
33. Forehand, D.I., Goldsmith, C.L. (2005) Wafer level micropackaging for RF MEMS switches. ASME InterPACK '05 Tech Conf, San Francisco, CA, July 2005.

http://www.springer.com/978-1-4419-6017-7

MEMS Reliability

Hartzell, A.L.; da Silva, M.G.; Shea, H.

2011, XIII, 291 p., Hardcover
ISBN: 978-1-4419-6017-7